Short Article

Structure

Expanding the PP2A Interactome by Defining a B56-Specific SLiM

Graphical Abstract

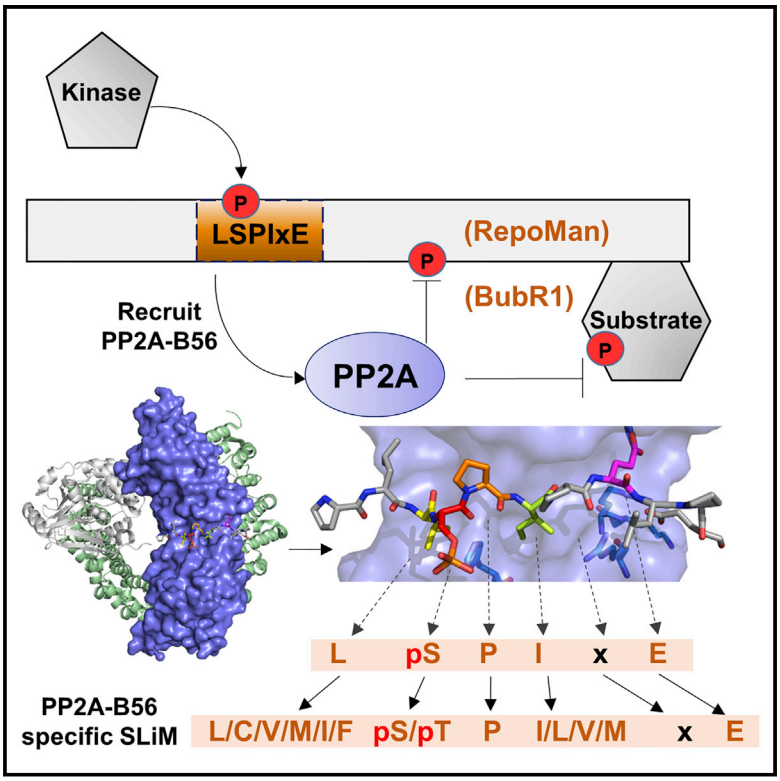

Authors

Xinru Wang, Rakhi Bajaj, Mathieu Bollen, Wolfgang Peti, Rebecca Page

Correspondence

rebecca_page@brown.edu

In Brief

Wang et al. report that BubR1 and RepoMan bind directly to PP2A-B56 using an LSPIxE short linear motif (SLiM), where phosphorylation of the Ser residue enhances binding. Using this SLiM motif, the authors identify more than 100 other potential PP2A targeting proteins and/or substrates.

Highlights

- Crystal structures of PP2A B56 in complex with phosphorylated RepoMan and BubR1
- RepoMan and BubR1 bind B56 using both hydrophobic and electrostatic interactions
- The PP2A-B56 specific short linear motif is L-*pS*-P-I-x-E
- The identification of more than 100 proteins that likely bind PP2A via this motif

Accession Numbers

5K6S
5SW9
5SWF

Wang et al., 2016, Structure *24*, 1–8
December 6, 2016
http://dx.doi.org/10.1016/j.str.2016.09.010

CellPress

Please cite this article in press as: Wang et al., Expanding the PP2A Interactome by Defining a B56-Specific SLiM, Structure (2016), http://dx.doi.org/10.1016/j.str.2016.09.010

Structure
Short Article

CellPress

Expanding the PP2A Interactome by Defining a B56-Specific SLiM

Xinru Wang,[1] Rakhi Bajaj,[1] Mathieu Bollen,[2] Wolfgang Peti,[3,4] and Rebecca Page[1,5,*]
[1]Department of Molecular Biology, Cell Biology and Biochemistry, Brown University, Providence, RI 02912, USA
[2]Laboratory of Biosignaling & Therapeutics, Department of Cellular and Molecular Medicine, KU Leuven, 3000 Leuven, Belgium
[3]Department of Molecular Pharmacology, Physiology and Biotechnology
[4]Department Chemistry
Brown University, Providence, RI 02912, USA
[5]Lead Contact
*Correspondence: rebecca_page@brown.edu
http://dx.doi.org/10.1016/j.str.2016.09.010

SUMMARY

Specific interactions between proteins govern essential physiological processes including signaling. Many enzymes, especially the family of serine/threonine phosphatases (PSPs: PP1, PP2A, and PP2B/calcineurin/CN), recruit substrates and regulatory proteins by binding short linear motifs (SLiMs), short sequences found within intrinsically disordered regions that mediate specific protein-protein interactions. While tremendous progress had been made in identifying where and how SLiMs bind PSPs, especially PP1 and CN, essentially nothing is known about how SLiMs bind PP2A, a validated cancer drug target. Here we describe three structures of a PP2A-SLiM interaction (B56:*pS*-RepoMan, B56:*pS*-BubR1, and B56:*pSpS*-BubR1), show that this PP2A-specific SLiM is defined as LSPIxE, and then use these data to discover scores of likely PP2A regulators and substrates. Together, these data provide a powerful approach not only for dissecting PP2A interaction networks in cells but also for targeting PP2A diseases, such as cancer.

INTRODUCTION

The serine/threonine Protein Phosphatase 2A (PP2A) recruits two distinct regulatory subunits (an A and a B subunit, the latter being either PR55 [B], B56 [PR61, B′], PR72 [B″], or PR93/PR110 [B‴]) to form highly selective holoenzymes (Shi, 2009). However, how these PP2A holoenzymes recruit substrates or are targeted to substrate-containing compartments is poorly understood. The serine/threonine protein phosphatases 1 and 2B (PP1; PP2B or calcineurin/CN) bind substrates and regulatory proteins using short functional sequences known as short linear motifs (SLiMs) (Peti and Page, 2015; Roy and Cyert, 2009). These SLiMs are found within intrinsically disordered regions (IDRs) of substrates and regulatory proteins and mediate specific protein-protein interactions (Ragusa et al., 2010). Sequence differences in and around the SLiM alter the binding affinity for a single anchoring site on binding partners, e.g., kinases or phosphatases (Nygren and Scott, 2015). Furthermore, SLiMs are also regulated by posttranslational modifications, e.g., phosphorylation, which alters their ability to bind their cognate binding partners (Kim et al., 2003). Together, these differences allow for a highly dynamic regulation of signaling pathways via SLiM interactions.

SLiMs have been identified in substrates and regulatory proteins of PP1 (RVxF, ΦΦ, SILK) and calcineurin (LxVP, PxIxIT, AID). Furthermore, subsequent structural studies have revealed how and where these SLiMs bind their respective phosphatases (Choy et al., 2014; Grigoriu et al., 2013; Hurley et al., 2007; Li et al., 2007; Terrak et al., 2004). It is now established that these SLiM interactions are essential for PSP function and signal fidelity. Indeed, it was recently shown that the blockbuster immunosuppressant drugs FK506 and cyclosporin A inhibit CN activity by binding the LxVP SLiM interaction pocket; i.e., they block substrate binding and, as a consequence, dephosphorylation (Grigoriu et al., 2013; Jin and Harrison, 2002). Thus, SLiM interaction sites are compelling drug targets as it is the interaction of folded enzymes and unfolded SLiMs that control many signaling pathways in the cell.

Recently, the first SLiM specific for PP2A was identified in the kinase BubR1 and the nuclear scaffolding protein RepoMan (Figure S1A) (Kruse et al., 2013; Qian et al., 2013; Suijkerbuijk et al., 2012; Xu et al., 2013). These studies demonstrated that BubR1 residues 662–682 and RepoMan residues 581–599, each of which includes a short LSPI motif surrounding a Cdk1 phosphorylation site ($S670_{BR1}$; $S591_{RM}$), are necessary for recruiting PP2A-B56. Although phosphorylation of these serines enhances PP2A-B56 recruitment by both proteins, there are conflicting data regarding the role of additional BubR1 phosphorylation sites ($S676_{BubR1}$; $T680_{BubR1}$) for B56 binding, as these sites are not conserved in RepoMan. Because mutations that disrupt B56 engagement lead to abnormal chromosome congression and segregation (BubR1) (Xu et al., 2013) and mitotic chromosome targeting (RepoMan) (Qian et al., 2013), it is now clear that this PP2A-specific SLiM interaction is critical for cell-cycle regulation. However, where this SLiM binds B56 and the role, if any, of residues outside the LSPI sequence in B56 binding is unknown.

Here we address these outstanding questions by determining the structures of three B56:LSPI complexes. The structures

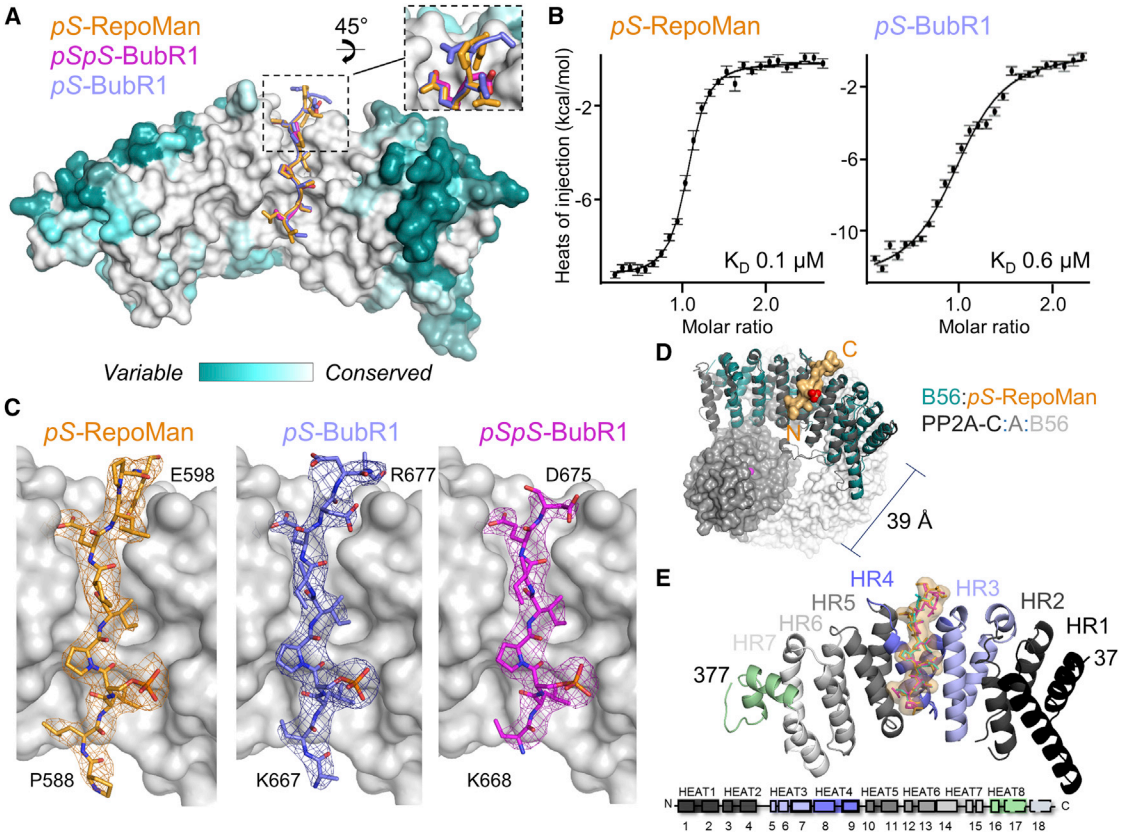

Figure 1. Structures of the B56:BubR1 and B56:RepoMan Complexes

(A) *pS*-RepoMan (orange), *pS*-BubR1 (light blue), and *pSpS*-BubR1 (magenta) bind B56 (surface colored according to sequence conservation).

(B) Binding isotherms of *pS*-RepoMan and *pS*-BubR1 with B56.

(C) Electron density of the *pS*-RepoMan, *pS*-BubR1, and *pSpS*-BubR1 peptides ($2F_o$-F_c, $\sigma = 1.0$).

(D) B56:*pS*-RepoMan complex (teal:orange) is superimposed on the B56 subunit in PP2A (PDB: 3FGA; catalytic domain, gray; A subunit, white; B56, dark gray). The distance between the PP2A catalytic center (Mn^{2+} ions in magenta) and the *pS* residue (red) in the LSPIxE motif is illustrated.

(E) BubR1/RepoMan peptides (orange surface; sticks colored as in C) bind B56 between heat repeats 3 and 4 (lavender and blue). B56 heat repeat schematic, with the corresponding helices numbered.

See also Figures S1 and S2; Tables S1 and S2.

identify the LSPI binding pocket on B56 and explain why serine phosphorylation is essential for binding. They also reveal that the SLiM is longer: LSPIxE. By using this expanded SLiM definition, we identified nearly 100 PP2A:B56 interactors, substantially expanding the B56 and, in parallel, the PP2A interactome. As SLiM binding pockets on phosphatases have been successfully targeted by Food and Drug Administration-approved drugs (i.e., FK506 and cyclosporin A, which target CN), a detailed molecular understanding of this site on PP2A-B56 will provide opportunities for the development of PP2A-specific therapeutics for cancer.

RESULTS

BubR1 and RepoMan LSPI-Containing Peptides Bind Directly to B56

To determine how BubR1 and RepoMan recruit PP2A:B56, we determined three crystal structures (Figure 1A and Table 1): (1) B56:*pS*-BubR1 (2.79 Å, monophosphorylated BubR1, ^{663}TLSIKKL-*pS*-PIIED*D*REA*D*H^{681}: *D* are S/T→D mutations that mimic phosphorylation and residues underlined are observed in the electron density and thus modeled); (2) B56:*pSpS*-BubR1 (2.82 Å, dually phosphorylated BubR1, ^{668}KL-*pS*-PIIED-*pS*^{676}); and (3) B56:*pS*-RepoMan (2.85 Å, monophosphorylated RepoMan, ^{581}RDIASKKPLL-*pS*-PIPELPEVPE^{601}). The SLiM-containing peptides bind B56 with K_D values of 0.6, 2.0, and 0.1 μM, respectively (by isothermal titration calorimetry [ITC]; Figure 1B and Table S1). Electron density (Figure 1C) for the bound peptides was evident in the initial molecular replacement maps. The structures of B56 in all three complexes are nearly identical to the free (Magnusdottir et al., 2009) and holoenzyme bound (Xu et al., 2009) structures (root-mean-square deviation [RMSD] of ~0.5 Å and ~0.8 Å, respectively; Figure S1B). The largest differences are observed in amino acids 51–64, which adopt a distinct conformation in the three B56:peptide complexes due to crystal contacts. Consistent with other B56 structures, no electron density was observed for B56 residues 110–127 (Magnusdottir et al., 2009). Finally, as expected, the BubR1/RepoMan binding pocket on B56 is fully accessible within the context of the PP2A-B56 holoenzyme (Figure 1D).

Table 1. Data Collection and Refinement Statistics

	B56:*pS*-RepoMan[a,b]	B56:*pS*-BubR1[a,c]	B56:*pSpS*-BubR1[a,d]
Data Collection			
Space group	P 2_1 2_1 2_1	P 2_1 2_1 2_1	P 2_1 2_1 2_1
Cell dimensions			
a, *b*, *c* (Å)	53.6, 109.0, 120.0	53.2, 107.8, 118.0	53.3, 107.4, 117.7
α, β, γ (°)	90, 90, 90	90, 90, 90	90, 90, 90
Resolution (Å)	38.21–2.85 (3.00–2.85)[e]	39.52–2.79 (2.94–2.79)[e]	39.51–2.82 (2.97–2.82)[e]
R_{merge}	0.097 (0.885)	0.072 (1.382)	0.075 (0.894)
Mean $I/\sigma I$	13.0 (2.0)	16.8 (1.7)	13.5 (1.8)
Completeness (%)	99.3 (97.3)	98.4 (93.2)	98.7 (93.8)
Multiplicity	5.5 (5.6)	6.6 (6.7)	5.3 (5.3)
$CC_{1/2}$	0.998 (0.686)	0.999 (0.625)	0.998 (0.686)
Refinement			
Resolution (Å)	38.21–2.85	39.52–2.79	39.52–2.82
No. of reflections	16,968	17,130	16,683
R_{work}/R_{free}	0.198/0.227	0.198/0.227	0.208/0.231
No. of atoms			
Protein	2,768	2,771	2,738
Water	23	10	13
B factors			
Protein	66.4	86.7	75.5
Water	60.4	78.5	75.2
RMSDs			
Bond lengths (Å)	0.002	0.002	0.002
Bond angles (°)	0.651	0.686	0.730
Ramachandran			
Outliers (%)	1.2	0.3	0.6
Allowed (%)	2.4	3.3	4.0
Favored (%)	96.4	96.4	95.4
Clashscore	1.63	1.45	2.20
PDB ID	5SW9	5K6S	5SWF

[a]Data were collected from a single crystal.
[b]*pS*-RepoMan, ^{581}RDIASKKPLL(pS)PIPELPEVPE^{601}.
[c]*pS*-BubR1, ^{663}TLSIKKL(pS)PIIEDDREADH^{681}.
[d]*pSpS*-BubR1, ^{668}KL(pS)PIIED(pS)^{676}.
[e]Values in parentheses represent the highest-resolution shell.

BubR1 and RepoMan Bind B56 in a Highly Conserved Pocket between the Third and Fourth HEAT Repeats

Both BubR1 and RepoMan bind B56 in an extended conformation at the center of the concave surface defined by the C-terminal helices of the B56 HEAT repeats 3 and 4 (Figure 1E). The interaction is extensive, burying ~1,200 Å^2 of solvent-accessible surface area in the three complexes, ~25% larger than that observed for other well-established SLiM interactions (Grigoriu et al., 2013). The BubR1/RepoMan residues that interact most extensively with B56 are L669$_{BR1}$/L590$_{RM}$, pS670$_{BR1}$/pS591$_{RM}$, I672$_{BR1}$/I593$_{RM}$, and E674$_{BR1}$/E595$_{RM}$ (Table S2). Notably, the B56 residues that interact directly with BubR1/RepoMan are conserved among all B56 isoforms (Figures 1A and S1C), explaining why both proteins bind equally effectively to all B56 isoforms in vivo (Qian et al., 2013; Suijkerbuijk et al., 2012; Xu et al., 2013).

The complexes show that B56 binds BubR1 and RepoMan using both hydrophobic (Figures 2A and S3) and electrostatic/polar interactions (Figures 2B, 2C, and S3). LSPI residues L669$_{BR1}$/L590$_{RM}$ and I672$_{BR1}$/I593$_{RM}$ bind into two adjacent hydrophobic pockets. The "Leu" binding pocket is defined by K183$_{B56}$, T184$_{B56}$, H187$_{B56}$, R188$_{B56}$, E226$_{B56}$, and I227$_{B56}$ (Figure 2A, lower panel) while the "Ile" binding pocket, which is deeper and ideally shaped to bind Ile residues, is defined by H187$_{B56}$, Y190$_{B56}$, I227$_{B56}$, and I231$_{B56}$ (Figure 2A, middle panel). These interactions are essential for binding, as mutating these residues to alanine (ASPA; or LSPA) in either BubR1 or RepoMan abolishes B56 binding (Kruse et al., 2013; Qian et al., 2013).

These hydrophobic interactions optimally position the phosphorylated serines of the three peptides to project away from the surface of B56 and form bidentate salt bridges with R188$_{B56}$ (Figures 2A and 2B, lower panel). This allows H187$_{B56}$

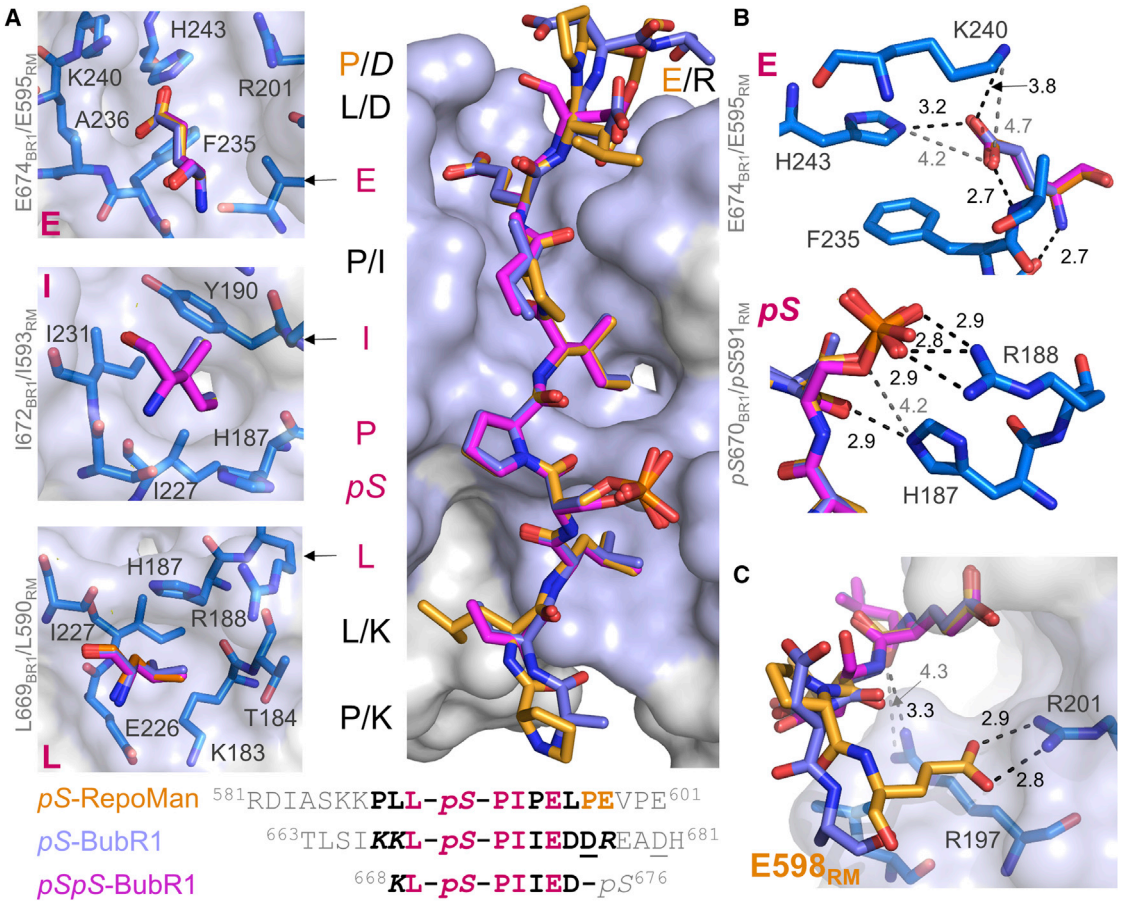

Figure 2. The PP2A:B56-Specific SLiM Is LSPIxE

(A) The B56 binding pocket (lavender) with *pS*-RepoMan (orange), *pS*-BubR1 (light blue), and *pSpS*-BubR1 (magenta); LSPIxE residues in dark pink and the RepoMan residues that make additional B56 contacts in orange; residues not conserved between the peptides are written as RepoMan/BubR1. The B56 residues (blue) that constitute the LSPIxE L, I, and E pockets are shown in the left panels. The peptide sequences used for complex formation are shown below: gray, not modeled due to lack of density; bold, modeled residues; dark pink, residues conserved between the peptides; orange, RepoMan residues that define the E598 pocket (see C); italics, side chains not modeled; underline, phosphomimetic mutations.

(B) Electrostatic and H-bond interactions between the pS residues and the E residues of the LSPIxE motif; colored as in (A). Electrostatic and H-bond interactions are shown as dashes (black, ≤4.0 Å; gray, ≤5.0 Å) with the distances in angstroms provided.

(C) The $E598_{RM}$ binding pocket that is specific to RepoMan, colored as in (A). Electrostatic and H-bond interactions as in (B).

See also Figure S3.

to form hydrogen bonds with the $pS670_{BR1}$/$pS591_{RM}$ carbonyl, restraining the bound peptides. Although the $P671_{BR1}$/$P592_{RM}$ side chains point up and away from B56, they play an important structural role by directing the BubR1/RepoMan peptide chains back toward B56, allowing $I672_{BR1}$/$I593_{RM}$ to bind into the deep "Ile" hydrophobic pocket. $P671_{BR1}$/$P592_{RM}$ are also required for the efficient phosphorylation of $S670_{BubR1}$/$S591_{RM}$ by CDK1 (its kinase motif is S/T-P), an event that strongly enhances the binding of this SLiM to B56. Finally, $R197_{B56}$ further restrains the orientation of the BubR1/RepoMan peptides by forming a hydrogen bond with the carbonyl of $Ile673_{BubR1}$ (Figure 2C).

Unexpectedly, we also observed a third salt bridge between $E674_{BR1}$/$E595_{RM}$ and both $K240_{B56}$ and $H243_{B56}$ (Figure 2B, upper panel). This interaction allows $E674_{BR1}$/$E595_{RM}$ to bind a third deep pocket in B56 defined by $F235_{B56}$, $K240_{B56}$, and $H243_{B56}$ (Figure 2A, upper panel). As a consequence, $E674_{BR1}$/$E595_{RM}$ are two of the most buried peptide residues in the B56 complexes (Table S2), suggesting that this interaction is critical for B56 binding. This was confirmed by peptide binding studies which showed that mutating this residue to an alanine weakens the affinity of BubR1 for B56 to levels nearly identical to that observed by mutating either the "L" or "I" in the LSPI motif to an alanine (Kruse et al., 2013). Together, these data demonstrate that the PP2A-B56 specific SLiM corresponds to an LSPIxE motif, with phosphorylation of the "S" residue enhancing binding via key electrostatic interactions with B56.

RepoMan Binds to B56 Using an Extended LSPIxE Motif, LSPIxExPE

Our structures revealed multiple, prominent electrostatic interactions between BubR1/RepoMan and B56. To understand the importance of the electrostatic interactions for binding, we used ITC (for summarized ITC data, see Table S1 and Figure S2). We first measured the affinity between BubR1 and B56 at

different salt concentrations (300–150 mM; increasing concentrations of salt weaken the strength of electrostatic interactions due to ionic shielding). The binding affinity of BubR1 ^{668}KLpSPIIEDE^{676} for B56 increases by ~3.6-fold as the salt concentration is reduced, confirming the importance of electrostatics for overall binding strength. We then tested the role of specific ionic interactions. The most prominent interaction is that mediated by pS670$_{BR1}$/pS591$_{RM}$, which binds H187$_{B56}$ and R188$_{B56}$. Previous work showed that in vivo substitution of the anchoring pS residue with a D is not phosphomimicking (Qian et al., 2015). Our structures reveal why this is the case: an Asp is too short to effectively reach the R188$_{B56}$ side chain. However, the structures suggested that an E would also not be phosphomimicking. This is because three of the four pS670 oxygens mediate ionic interactions, something not possible with either a Glu or Asp (Figure 2B, lower panel). As hypothesized, substituting E for pS (^{668}KL*p*SPIIEDE^{676} versus ^{668}KLEPIIEDE^{676}) weakens the affinity for B56 by 2.4-fold. This demonstrates that although D and E are often used to mimic phosphorylated residues, neither are suitable mimics for the pS residue in the PP2A-B56-specific LSPIxE motif. A recent study confirms that a S670E$_{BR1}$ substitution does not function as a phosphorylation mimic for defining this interaction (Wang et al., 2016).

We then tested the role of residues outside the LSPIxE SLiM for binding. Phosphorylation of a BubR1 residue C-terminal to the LSPIxE motif, S676$_{BR1}$, has been suggested to be important for B56 binding even though this serine is not conserved in RepoMan (the corresponding residue is P597$_{RM}$). Our structures show that neither the S676D$_{BR1}$ (*pS*-BubR1) nor the *pS*676$_{BR1}$ (*pSpS*-BubR1) residue makes significant contacts with B56, suggesting that this residue does not significantly contribute to binding. We tested this using ITC (Table S1 and Figure S2). The data showed that, unlike pS670$_{BR1}$, pS676$_{BR1}$ can be substituted by Glu without affecting binding affinity for B56 (^{668}KL*p*SPIIEDE^{676} versus ^{668}KL*p*SPIIED*p*S^{676}). Furthermore, removing this residue altogether only modestly weakens binding, reducing it by ~1.7-fold (^{668}KL*p*SPIIED^{675}).

The peptides used for these ITC measurements constitute the structurally determined core LSPIxE motif. However, we also performed ITC measurements with a longer peptide (Table S1). This peptide exhibited ~3-fold stronger binding. This affinity increase is due largely to a ~35% reduction in entropy, likely due to the different amino acid composition and/or the different chain length of the peptide. We then repeated the ITC with the longer phosphorylated RepoMan LSPIxE peptide. This peptide bound B56 ~5-fold more strongly than the longer BubR1 peptide. This increase in affinity was due, in part, to a large reduction in entropy compared to BubR1. However, it was also due to direct interactions between B56 and RepoMan not observed in either of the B56:BubR1 complexes. Namely, RepoMan, but not BubR1, forms an additional bidentate salt bridge between E598$_{RM}$ and R201$_{B56}$ (Figure 2C). Together, these data demonstrate the importance of both enthalpic and entropic contributions to the overall binding energies between IDR SLiMs and their folded protein binding partners. They also demonstrate how residues outside the core LSPIxE SLiM of distinct B56 regulators and substrates function to fine-tune their affinities for B56.

Using the LSPIxE SLiM to Identify B56 Interactors

Our structures of the three B56:LSPIxE complexes, in conjunction with appropriate secondary filters, can now be leveraged to define the PP2A SLiM motif(s) that will successfully identify PP2A interacting proteins. This is complementary to a sequence conservation and computational prediction approach that was recently used to identify LSPI sequences (Hertz et al., 2016). By using these structures as a "molecular ruler" to define the LSPIxE SLiM, we focus on identifying the most stringent B56 interactors.

Using the structurally determined LSPIxE SLiM and ScanProsite (de Castro et al., 2006), we identified 13 instances (sites) of this motif in 13 different human proteins, ~90% fewer than using the LSPI definition alone (Figure 3A; Tables S3 and S4). Because the LSPIxE motif in both BubR1 and RepoMan are present in IDRs (required for the extended binding observed in the B56:BubR1 complex) and because phosphorylation significantly enhances binding, we applied two additional secondary filters: (1) multiple disorder prediction algorithms to ensure the identified sites are in IDRs and (2) NetPhos (Blom et al., 1999) to ensure sites are phosphorylated. Applying these filters identified ten LSPIxE sites in ten distinct proteins (Figure 3B and Table S3). Thus, we predict that these ten proteins bind directly to PP2A:B56 and do so in a manner identical to that observed for BubR1 and RepoMan. Interestingly, as is true of BubR1 and RepoMan, 60% of the identified potential B56 interacting proteins are present in the nucleus, correlating well with the essential role of PP2A during the cell cycle.

It is immediately apparent, however, that this strict definition of the LSPIxE SLiM will fail to detect PP2A interactors that have similar, yet also binding compatible sequences. We analyzed the B56:LSPIxE structures to identify amino acids that can be accommodated in the Leu and Ile binding pockets; i.e., we used the B56 structures as a rigid geometric ruler. This approach is valid, as these pockets are unchanged between the three B56 complexes (Figure 1A) and in the structures of B56 alone and the PP2A:B56 holoenzyme (Figure S1B). The Leu binding pocket is larger and less well defined than the Ile binding pocket (Figure 2A, lower panel) and thus can accommodate a Val, Met, or Cys and, with some small B56 side-chain rearrangements, an Ile or a Phe. Trp and Tyr residues are excluded as they are too bulky to fit into the pocket. Similarly, polar and charged residues are excluded as there are no amino acids in the pocket positioned to mediate compensatory polar interactions. Expanding the motif to include these additional residues modestly increases the number of sites and proteins identified ([LCVMIF]-SPIxE, 20 sites in 19 proteins; Figure 3A and Table S4). Interestingly, RepoMan, a protein with a confirmed B56-specific LSPIxE SLiM, is predicted to have two LSPIxE sites using this expanded motif (^{590}LSPIpE^{595}, confirmed; ^{935}MSPIkE^{940}, discovered in this analysis). This gives rise to the intriguing possibility that these distal sites might be activated by phosphorylation via distinct kinases at different times during the cell cycle and thereby differentially regulate PP2A targeting during mitosis.

In contrast to the open Leu binding pocket, the Ile binding pocket is more constrained (Figure 2A, middle panel). An analysis of the binding pocket suggests that a Leu, Met, and Val can also be accommodated at this site; as with the Leu binding pocket, larger amino acids and charged/polar amino acids are

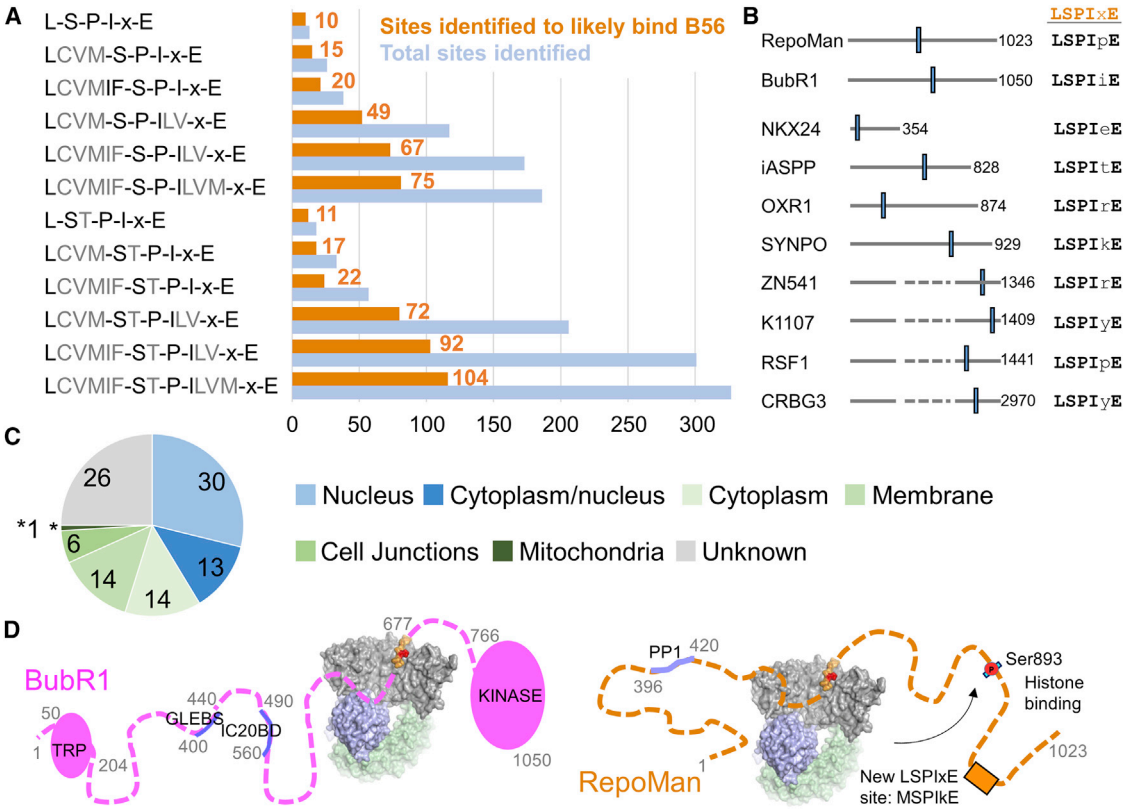

Figure 3. Potential PP2A:B56 LSPIxE Interactors

(A) Bar graph illustrating the number of motifs identified in the human UniProt database using listed motifs. Blue, total sites identified; orange, "likely interactors," i.e., sequences that are (1) predicted to be in IDRs and (2) predicted to be phosphorylated.

(B) Gene names and schematics of the ten human proteins with LSPIxE sites.

(C) Cellular localization of the likely interactors of B56.

(D) Models of the PP2A-B56:BubR1 and PP2A-B56:RepoMan complexes; S893 is dephosphorylated by PP2A-B56.

See also Tables S3, S4 and S5.

too bulky or charged, respectively, to effectively bind this pocket without significant structural rearrangements, an observation consistent with previous mutagenesis data (Qian et al., 2013). Combining our expanded definition of the Leu binding site with the Ile binding site results in a much greater number of sites identified: 75 [LCVMIF]-SP-[ILVM]-xE sites (Figure 3A and Table S4). Allowing the phosphorylated residue to be either a Ser or Thr further increases the number of sites identified by ~30%: 104 [LCVMIF]-[ST]-P-[ILVM]-xE sites (Figure 3A; Tables S4 and S5). Although the application of these strict geometric rules and filters may not capture all interactors, it identifies those most likely to bind in the B56 LSPIxE SLiM binding pocket.

Strikingly, as for the ten sites identified using the strict definition of the motif (LSPIxE), nearly half of the sites using the expanded definition are in nuclear proteins (Figure 3C). Several of the identified proteins have already been associated with PP2A in vivo or shown to have roles in cell division, a process in which PP2A activity is vital (Table S5). For example, Kif4A interacts directly with PP2A B56 subunits (Bastos et al., 2014). Our analysis identified a ^{1224}CSPIeE^{1229} SLiM sequence near the C terminus of Kif4A (^{1226}CSPIeE^{1231} in Kif4B). Furthermore, studies have shown that Ser1125$_{Kif4A}$ is phosphorylated during mitosis (Dephoure et al., 2008). Our analysis strongly suggests that Kif4A binds directly to PP2A:B56 via this LSPIxE SLiM. We also discovered that well-known mitotic proteins also contain LSPIxE sites, and thus likely also target PP2A during the cell cycle. For example, RepoMan has two LSPIxE sequences; given that Ser936$_{RM}$ has already been identified to be phosphorylated (Rigbolt et al., 2011), it is likely that ^{935}MSPIkE^{940} also binds and targets PP2A. Most intriguing in relation to BubR1 is the identification of LSPIxE sites in both Bub1 (^{654}FSPIqE^{659}) and KNL1 (^{1041}LTPLeE^{1046}). This is of interest, as KNL1 is a scaffold for both Bub1 and BubR1 and our findings suggest that all three proteins may function to target PP2A to kinetochores during mitosis.

DISCUSSION

In contrast to protein tyrosine phosphatases (PTPs), identifying PSP substrates, especially those of PP1 and PP2A, has been comparatively difficult. This is because the approaches for identifying substrates of PTPs, including non-covalent substrate-trapping mutants (Flint et al., 1997) and selective inhibitors (Honkanen et al., 1994), are much less developed for PP1 and PP2A. It is for these reasons that it has been especially challenging to identify bona fide substrates of PP2A, PP1, and CN

and, as a consequence, to fully elucidate the roles of PSPs in distinct signaling cascades. The identification of SLiMs that are specific for these PSPs provides the first steps to overcome this difficulty.

Our structures reveal that LSPIxE defines a PP2A-specific SLiM, with all five residues in the SLiM mediating key interactions with B56. In particular, the "E" in the LSPIxE SLiM interacts extensively with $H243_{B56}$. This is of special interest, as the B56 H243P mutation has been identified in embryonal carcinoma tumors (Nobumori et al., 2013). The structures also explain why the phosphorylation of the "S" residue enhances binding to B56; it mediates key electrostatic interactions with $H187_{B56}$ and $R188_{B56}$ in B56. This differs from PP1-specific SLiMs (RVxF, SILK, among others), where phosphorylation reduces PP1 binding (Kim et al., 2003). The differential response of PSPs to the phosphorylation state of their specific SLiMs allows PSPs to associate with discrete regulators at different times to direct distinct biological outcomes.

Most importantly, the discovery that the PP2A-specific SLiM is LSPIxE also led to the identification of 104 instances of this motif in 98 human proteins that are potential PP2A interactors (Figure 3A and Table S5). Only a handful of these proteins were previously identified as PP2A targeting proteins, as they require specific cellular conditions, i.e., phosphorylation, to effectively engage PP2A. Whether the identified proteins function solely as targeting proteins, like BubR1, or also substrates, like RepoMan, remains to be determined (Figure 3D). Finally, these B56:SLiM structures also have important implications for the development of novel compounds that target PP2A. PSPs were generally considered to be undruggable because natural product inhibitors of PSP active sites are poorly selective and highly toxic. However, recent structural and functional studies are leading to the emerging view that PSP SLiM binding sites are highly targetable. For example, the LxVP SLiM binding pocket, which is used by scores of CN substrates to bind CN, is the binding site of the immunosuppressants FK506 and CSA; i.e., they potently inhibit CN by simply blocking the phosphatase from binding its substrates. It is now clear that a similar strategy can be used to target PP2A, thereby providing a powerful approach for both dissecting PP2A signaling pathways and targeting PP2A diseases, such as cancer.

EXPERIMENTAL PROCEDURES

Detailed protein expression, purification, crystallization, structure determination, and ITC methods can be found in Supplemental Experimental Procedures.

Structure Determination

$B56_{\gamma31–380}$ was purified using His-tag chromatography, tobacco etch virus cleavage and size-exclusion chromatography, and incubated with BubR1/RM peptides in a 1:5 molar ratio.

Crystals of the complexes grew in 0.1 M HEPES (pH 7.75), 0.8 M LiCl, and 8% polyethylene glycol (PEG) 6000 (B56:*pS*-BubR1) or 8% PEG 8000 (B56:*pSpS*-BubR1, B56:*pS*-RepoMan) using hanging-drop vapor diffusion at room temperature. Data were collected at Stanford Synchrotron Radiation Lightsource (SSRL) beamline 12.2 at 100 K and a wavelength of 0.98 Å using a Pilatus 6M PAD detector. The data were processed and the structures refined as described in Supplemental Experimental Procedures. Data collection and refinement details are provided in Table 1.

Bioinformatics

ScanProsite (de Castro et al., 2006) was used to identify additional PP2A interacting proteins that contain an LSPIxE SLiM. Definition of the search sequences was based on the experimental three-dimensional B56:*pS*-RepoMan, B56:*pS*-BubR1, and B56:*pSpS*-BubR1 complex structures. The probability of these proteins containing functional LSPIxE motifs (i.e., ones that bind B56 in the B56 LSPIxE motif binding grooves) was further evaluated by disorder prediction (method used described in detail in Supplemental Experimental Procedures) as it is well recognized that SLiMs are only identified in IDRs. Furthermore, as phosphorylation was experimentally shown to significantly enhance binding, NetPhos was used to select only hits with a high likelihood of being phosphorylated (NetPhos >0.5) (Blom et al., 1999).

ACCESSION NUMBERS

The accession number for the reported crystal structures are PDB: 5K6S (B56:*pS*-BubR1), PDB: 5SW9 (B56:*pS*-RepoMan), and PDB: 5SWF (B56:*pSpS*-BubR1).

SUPPLEMENTAL INFORMATION

Supplemental Information includes Supplemental Experimental Procedures, three figures, and five tables and can be found with this article online at http://dx.doi.org/10.1016/j.str.2016.09.010.

AUTHOR CONTRIBUTIONS

X.W, M.B, W.P. and R.P. conceived experiments and wrote the manuscript. X.W., R.B., W.P. and R.P performed and analyzed experiments. X.W, R.B. W.P., M.B and R.P. discussed the data and manuscript.

ACKNOWLEDGMENTS

The work was supported by NINDS (R01NS091336; W.P.) NIGMS (R01GM098482; R.P.), the Fund for Scientific Research-Flanders (G.0473.12, G.0482.12; M.B.), and a Flemish Concerted Research Action (GOA 15/016, M.B.). Some data were obtained at the BU Structural Biology Core Facility (BioMed, Brown University). Crystallographic data were collected at SSRL. Use of SSRL is supported by the US DOE, Office of Science, Office of Basic Energy Sciences under Contract DE-AC02-76SF00515. The SSRL Structural Molecular Biology Program is supported by the DOE Office of Biological and Environmental Research and by the NIH-NIGMS (P41GM103393).

Received: June 15, 2016
Revised: August 11, 2016
Accepted: October 3, 2016
Published: October 27, 2016

REFERENCES

Bastos, R.N., Cundell, M.J., and Barr, F.A. (2014). KIF4A and PP2A-B56 form a spatially restricted feedback loop opposing Aurora B at the anaphase central spindle. J. Cell Biol. *207*, 683–693.

Blom, N., Gammeltoft, S., and Brunak, S. (1999). Sequence and structure-based prediction of eukaryotic protein phosphorylation sites. J. Mol. Biol. *294*, 1351–1362.

Choy, M.S., Hieke, M., Kumar, G.S., Lewis, G.R., Gonzalez-DeWhitt, K.R., Kessler, R.P., Stein, B.J., Hessenberger, M., Nairn, A.C., Peti, W., et al. (2014). Understanding the antagonism of retinoblastoma protein dephosphorylation by PNUTS provides insights into the PP1 regulatory code. Proc. Natl. Acad. Sci. USA *111*, 4097–4102.

de Castro, E., Sigrist, C.J., Gattiker, A., Bulliard, V., Langendijk-Genevaux, P.S., Gasteiger, E., Bairoch, A., and Hulo, N. (2006). ScanProsite: detection of PROSITE signature matches and ProRule-associated functional and structural residues in proteins. Nucleic Acids Res. *34*, W362–W365.

Dephoure, N., Zhou, C., Villen, J., Beausoleil, S.A., Bakalarski, C.E., Elledge, S.J., and Gygi, S.P. (2008). A quantitative atlas of mitotic phosphorylation. Proc. Natl. Acad. Sci. USA *105*, 10762–10767.

Flint, A.J., Tiganis, T., Barford, D., and Tonks, N.K. (1997). Development of "substrate-trapping" mutants to identify physiological substrates of protein tyrosine phosphatases. Proc. Natl. Acad. Sci. USA *94*, 1680–1685.

Grigoriu, S., Bond, R., Cossio, P., Chen, J.A., Ly, N., Hummer, G., Page, R., Cyert, M.S., and Peti, W. (2013). The molecular mechanism of substrate engagement and immunosuppressant inhibition of calcineurin. PLoS Biol. *11*, e1001492.

Hertz, E.P., Kruse, T., Davey, N.E., Lopez-Mendez, B., Sigurethsson, J.O., Montoya, G., Olsen, J.V., and Nilsson, J. (2016). A conserved motif provides binding specificity to the PP2A-B56 phosphatase. Mol. Cell *63*, 686–695.

Honkanen, R.E., Codispoti, B.A., Tse, K., Boynton, A.L., and Honkanan, R.E. (1994). Characterization of natural toxins with inhibitory activity against serine/threonine protein phosphatases. Toxicon *32*, 339–350.

Hurley, T.D., Yang, J., Zhang, L., Goodwin, K.D., Zou, Q., Cortese, M., Dunker, A.K., and DePaoli-Roach, A.A. (2007). Structural basis for regulation of protein phosphatase 1 by inhibitor-2. J. Biol. Chem. *282*, 28874–28883.

Jin, L., and Harrison, S.C. (2002). Crystal structure of human calcineurin complexed with cyclosporin A and human cyclophilin. Proc. Natl. Acad. Sci. USA *99*, 13522–13526.

Kim, Y.M., Watanabe, T., Allen, P.B., Kim, Y.M., Lee, S.J., Greengard, P., Nairn, A.C., and Kwon, Y.G. (2003). PNUTS, a protein phosphatase 1 (PP1) nuclear targeting subunit. Characterization of its PP1- and RNA-binding domains and regulation by phosphorylation. J. Biol. Chem. *278*, 13819–13828.

Kruse, T., Zhang, G., Larsen, M.S., Lischetti, T., Streicher, W., Kragh Nielsen, T., Bjorn, S.P., and Nilsson, J. (2013). Direct binding between BubR1 and B56-PP2A phosphatase complexes regulate mitotic progression. J. Cell Sci. *126*, 1086–1092.

Li, H., Zhang, L., Rao, A., Harrison, S.C., and Hogan, P.G. (2007). Structure of calcineurin in complex with PVIVIT peptide: portrait of a low-affinity signalling interaction. J. Mol. Biol. *369*, 1296–1306.

Magnusdottir, A., Stenmark, P., Flodin, S., Nyman, T., Kotenyova, T., Graslund, S., Ogg, D., and Nordlund, P. (2009). The structure of the PP2A regulatory subunit B56 gamma: the remaining piece of the PP2A jigsaw puzzle. Proteins *74*, 212–221.

Nobumori, Y., Shouse, G.P., Wu, Y., Lee, K.J., Shen, B., and Liu, X. (2013). B56gamma tumor-associated mutations provide new mechanisms for B56gamma-PP2A tumor suppressor activity. Mol. Cancer Res. *11*, 995–1003.

Nygren, P.J., and Scott, J.D. (2015). Therapeutic strategies for anchored kinases and phosphatases: exploiting short linear motifs and intrinsic disorder. Front. Pharmacol. *6*, 158.

Peti, W., and Page, R. (2015). Strategies to make protein serine/threonine (PP1, calcineurin) and tyrosine phosphatases (PTP1B) druggable: achieving specificity by targeting substrate and regulatory protein interaction sites. Bioorg. Med. Chem. *23*, 2781–2785.

Qian, J., Beullens, M., Lesage, B., and Bollen, M. (2013). Aurora B defines its own chromosomal targeting by opposing the recruitment of the phosphatase scaffold Repo-Man. Curr. Biol. *23*, 1136–1143.

Qian, J., Beullens, M., Huang, J., De Munter, S., Lesage, B., and Bollen, M. (2015). Cdk1 orders mitotic events through coordination of a chromosome-associated phosphatase switch. Nat. Commun. *6*, 10215.

Ragusa, M.J., Dancheck, B., Critton, D.A., Nairn, A.C., Page, R., and Peti, W. (2010). Spinophilin directs protein phosphatase 1 specificity by blocking substrate binding sites. Nat. Struct. Mol. Biol. *17*, 459–464.

Rigbolt, K.T., Prokhorova, T.A., Akimov, V., Henningsen, J., Johansen, P.T., Kratchmarova, I., Kassem, M., Mann, M., Olsen, J.V., and Blagoev, B. (2011). System-wide temporal characterization of the proteome and phosphoproteome of human embryonic stem cell differentiation. Sci. Signal. *4*, rs3.

Roy, J., and Cyert, M.S. (2009). Cracking the phosphatase code: docking interactions determine substrate specificity. Sci. Signal. *2*, re9.

Shi, Y. (2009). Assembly and structure of protein phosphatase 2A. Sci. China C Life Sci. *52*, 135–146.

Suijkerbuijk, S.J., Vleugel, M., Teixeira, A., and Kops, G.J. (2012). Integration of kinase and phosphatase activities by BUBR1 ensures formation of stable kinetochore-microtubule attachments. Dev. Cell *23*, 745–755.

Terrak, M., Kerff, F., Langsetmo, K., Tao, T., and Dominguez, R. (2004). Structural basis of protein phosphatase 1 regulation. Nature *429*, 780–784.

Wang, J., Wang, Z., Yu, T., Yang, H., Virshup, D.M., Kops, G.J., Lee, S.H., Zhou, W., Li, X., Xu, W., et al. (2016). Crystal structure of a PP2A B56-BubR1 complex and its implications for PP2A substrate recruitment and localization. Protein Cell *7*, 516–526.

Xu, Z., Cetin, B., Anger, M., Cho, U.S., Helmhart, W., Nasmyth, K., and Xu, W. (2009). Structure and function of the PP2A-shugoshin interaction. Mol. Cell *35*, 426–441.

Xu, P., Raetz, E.A., Kitagawa, M., Virshup, D.M., and Lee, S.H. (2013). BUBR1 recruits PP2A via the B56 family of targeting subunits to promote chromosome congression. Biol. Open *2*, 479–486.

Structure, Volume *24*

Supplemental Information

Expanding the PP2A Interactome by Defining a B56-Specific SLiM

Xinru Wang, Rakhi Bajaj, Mathieu Bollen, Wolfgang Peti, and Rebecca Page

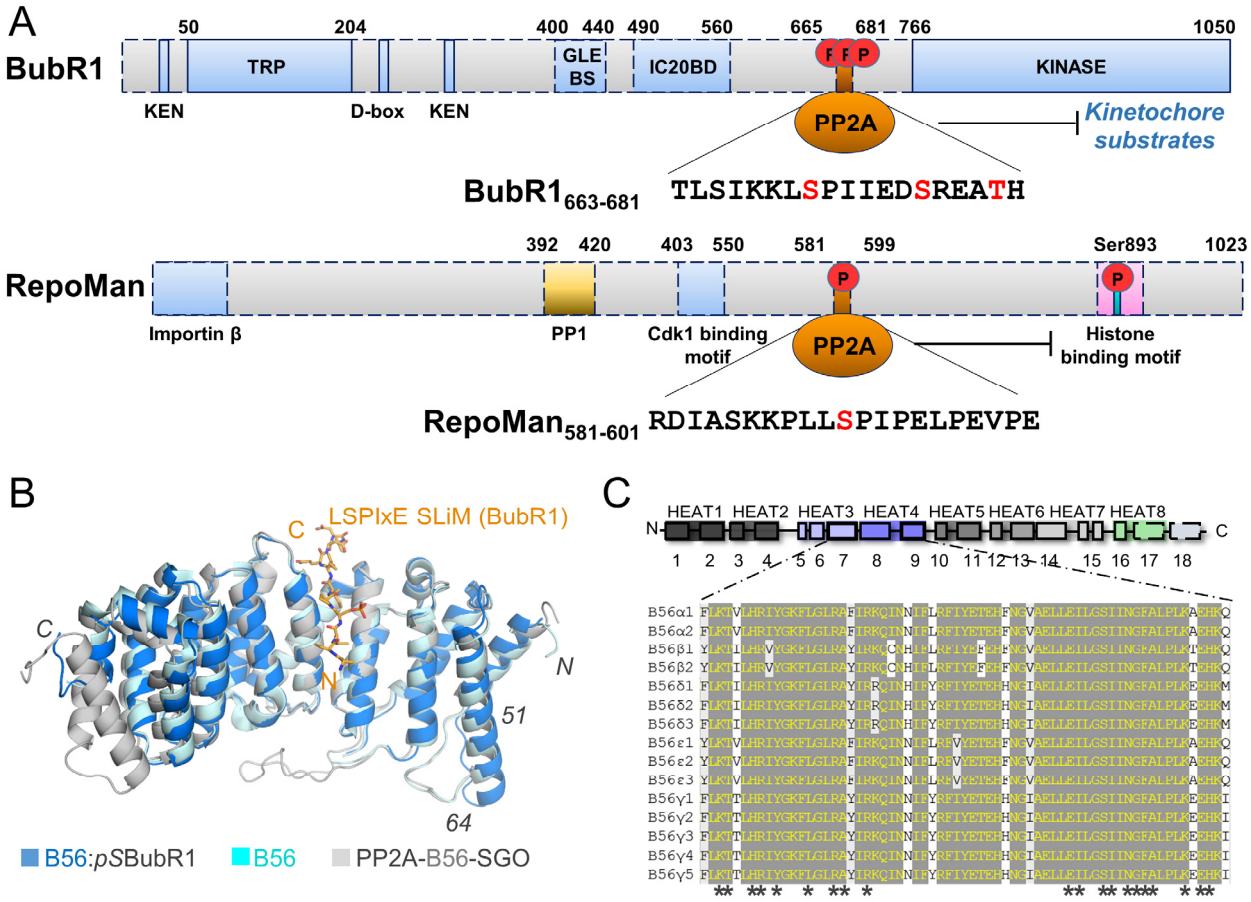

Figure S1. B56 targeting proteins and the overlay of distinct B56 complexes. Related to Figure 1.
(A) Domain structure of BubR1 and RepoMan; known protein interaction domains are indicated. Dotted lines indicate intrinsically disordered regions (IDRs); solid lines indicate folded domains. PP2A:B56 interaction sequence indicated.
(B) Overlay of B56 from the B56:*pS*BubR1 complex (blue) with free B56 (PDBID 2JAK; cyan) and B56 from the PP2A-B56-SGO complex (PDBID 3FGA; grey). Residue number 51-64 indicate the location of the loop that adopts a distinct conformation in the B56:*pS*RepoMan and B56:*pS*BubR1 complexes due to crystal contacts.
(C) Sequence alignment of the residues from B56 isoforms (homo sapiens) with the residues that constitute the LSPIxE binding pocket indicted by a '*'.

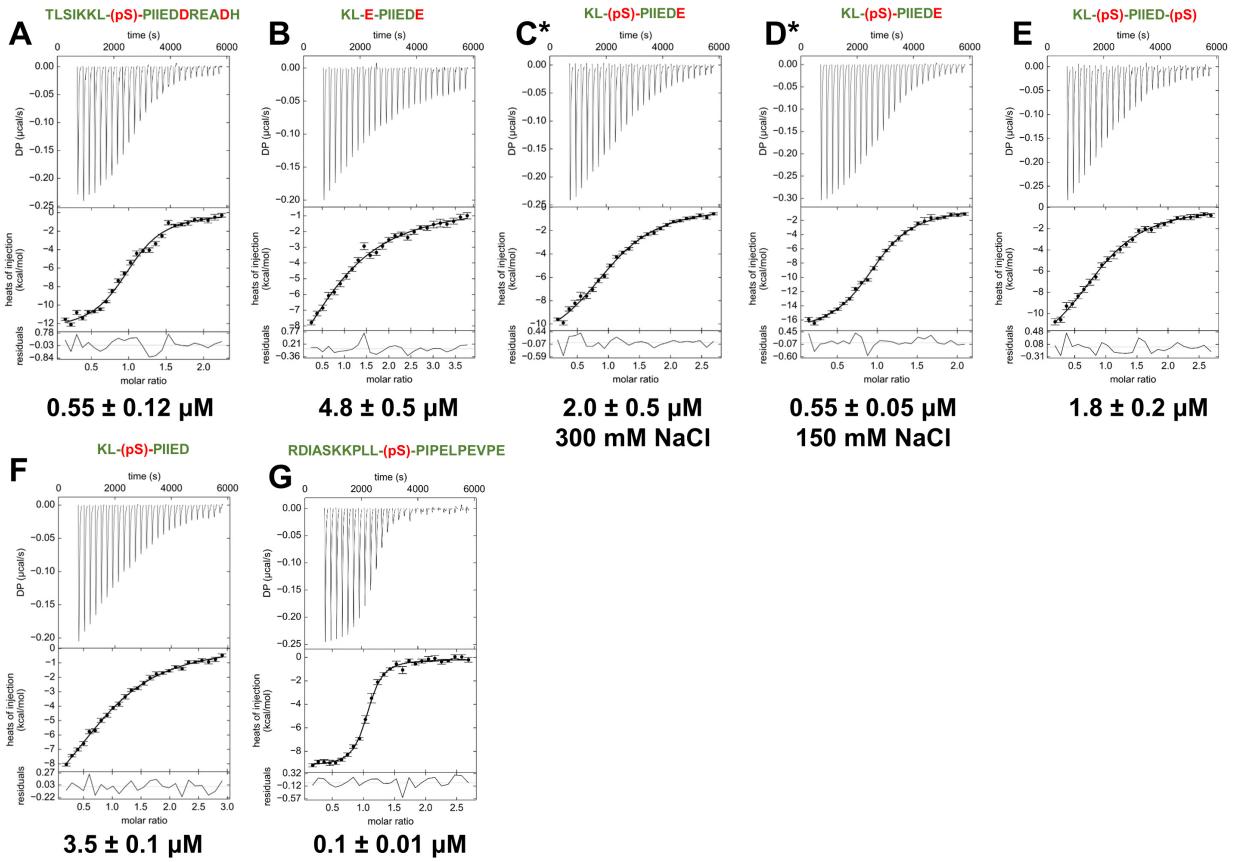

Figure S2. Isothermal titration calorimetry of LSPIxE peptides. **Related to Figure 1.**
(A) B56γ$_{12\text{-}380}$:BubR1 ^{663}TLSIKKL(pS)PIIED*D*REA*D*H^{681}
(B) B56γ$_{12\text{-}380}$:BubR1 ^{668}KLEPIIEDE^{676}
(C) B56γ$_{12\text{-}380}$:BubR1 ^{668}KL-(pS)-PIIEDE^{676}
(D) B56γ$_{12\text{-}380}$:BubR1 ^{668}KL-(pS)-PIIEDE^{676} , *low salt.*
(E) B56γ$_{12\text{-}380}$:BubR1 ^{668}KL-(pS)-PIIED(pS)^{676}
(F) B56γ$_{12\text{-}380}$:BubR1 ^{668}KL-(pS)-PIIED^{675}
(G) B56γ$_{12\text{-}380}$:RepoMan ^{581}RDIASKKPLL(pS)PIPELPEVPE^{601}.
All experiments performed in ITC buffer (50 mM sodium phosphate pH 7.5, 300 mM NaCl, 0.5 mM TCEP), with the exception of (D), which was performed in a low salt buffer (50 mM sodium phosphate pH 7.5, 150 mM NaCl, 0.5 mM TCEP). All measurements represent an n = 2 or 3.

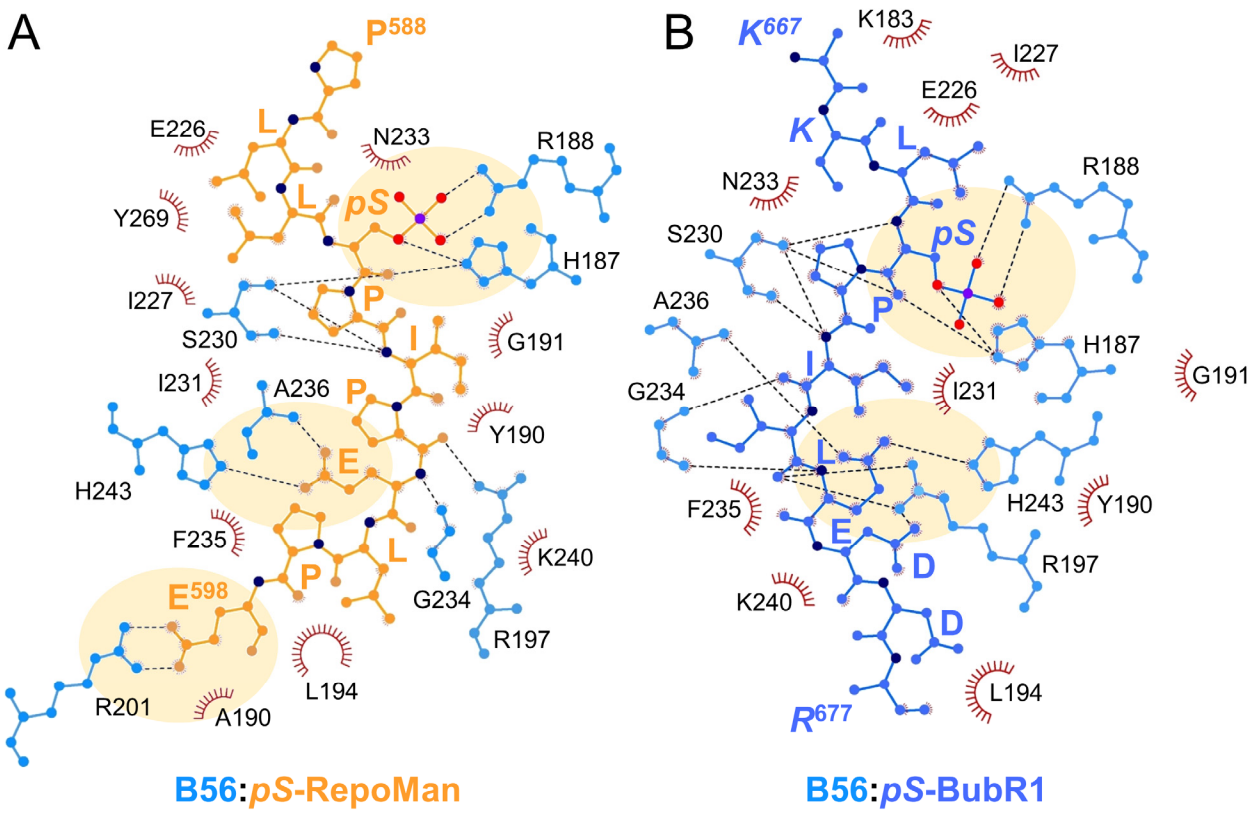

Figure S3. Ligplot figures of the hydrophobic and electrostatic/polar interactions between LSPIxE peptides and B56. Related to Figure 2.

(A) Ligplot diagram of the hydrophobic (red semi-circles) and electrostatic/polar interactions (dashed lines) between B56 (blue) and RepoMan (orange). B56 residues are labeled in black while RepoMan residues are in orange (^{588}PLL-*pS*-PIPELPE^{598}). Residues in key electrostatic interactions are highlighted by an orange circle.

(B) Ligplot diagram of the hydrophobic (red semi-circles) and electrostatic/polar interactions (dashed lines) between B56 (blue) and BubR1 (lavender). B56 residues are labeled in black while BubR1 residues are in blue (^{567}*KK*L-*pS*-PILEDD*R*^{677}; sidechains were not modeled for italicized residue labels due to a lack of density). Residues in key electrostatic interactions are highlighted by an orange circle.

Table S1: Isothermal titration calorimetry (ITC) measurements of PP2A-B56 with BuBR1 and RepoMan. Related to Figure 1.

B56	Peptides	K_D (μM)	ΔH (kcal/mol)	TΔS (kcal/Mol)
12-380	BUBR1 - ^{668}KLEPIIEDE^{676}	4.8 ± 0.5	-15.5 ± 0.8	-8.2 ± 0.7
12-380	BUBR1 - ^{668}KL-(pS)-PIIEDE^{676}	2.0 ± 0.5	-14.7 ± 1.6	-7.0 ± 1.8
12-380*	BUBR1 - ^{668}KL-(pS)-PIIEDE^{676}	0.55 ± 0.05	-17.6 ± 0.1	-9.1 ± 0.1
12-380	BUBR1 - ^{668}KL-(pS)-PIIED(pS)^{676}	1.8 ± 0.2	-13.8 ± 0.9	-6.0 ± 1.0
12-380	BUBR1 - ^{668}KL-(pS)-PIIED^{675}	3.5 ± 0.1	-14.5 ± 1.6	-7.1 ± 1.7
12-380	BUBR1 - ^{663}TLSIKKL(pS)PIIEDDREADH^{681}	0.55 ± 0.12	-12.9 ± 0.1	-4.4 ± 0.1
12-380	RepoMan - ^{581}RDIASKKPLL(pS)PIPELPEVPE^{601}	0.1 ± 0.01	-10.0 ± 0.9	-0.5 ± 1.0

All reported measurements are performed with ITC buffer (50 mM sodium phosphate pH 7.5, 300 mM NaCl, 0.5 mM TCEP). Errors are from duplicate or triplicate measurements

*Low salt ITC buffer: 50 mM sodium phosphate pH 7.5, 150 mM NaCl, 0.5 mM TCEP

Table S2: Residues that define the B56:BubR1 (LSPIxE) interface. Related to Figure 1.

B56°	**BSA^ (Å²)**	***pS*- BubR1***	**BSA (Å²)**	***pSpS*-BubR1***	**BSA (Å²)**	***pS*-RepoMan***	**BSA (Å²)**
Leu 194	63.0	**Ile 672**	147.9	**Ile 672**	147.1	**Ile 593**	148.9
His 187	60.2	**Glu 674**	142.6	**Leu 669**	136.2	**Leu 590**	131.7
Ser 230	54.4	**Leu 669**	135.1	**Glu674**	134.7	**Glu 595**	126.1
Gly 234	53.9	***p*Ser 670**	57.9	***p*Ser 670**	55.2	**Glu 598***	99.3
Arg 197	51.9	**Pro 671**	46.4	Asp 675	50.5	***p*Ser 591**	58.5
Glu 226	38.1	Arg 677	38.4	**Pro 671**	42.3	**Leu 589**	49.4
Arg 188	36.6	Asp 675	37.7	Ile 673	24.2	**Pro 592**	45.6
Asn 233	26.9	Lys 668	26.7	Lys 668	21.6	Leu 596	39.3
Lys 240	26.6	Ile 673	21.1			Pro 594	18.9
Ala 236	24.2	Asp 676	11.0			Pro 597	14.1
Tyr 190	16.4	Lys 667	6.1			Pro 588	5.3
Ile 231	14.9						
Tyr 269	14.5						
His 243	12.8						
Phe 235	11.9						
Lys 183	11.7						
Thr 184	11.2						
Gly 191	9.0						
Arg 201	8.8						
Gly 195	5.5						
Ile 227	2.9						

°Values of BSA for B56 residues obtained from the B56:pS-BubR1 complex
^BSA, buried solvent accessible surface area
*LSPI-E residues in bold; the RepoMan Glu residue (Glu 598) that makes an additional salt bridge with B56 is in red

Table S3: Human proteins with LSPIxE motifs. Related to Figure 3.

Protein*	Gene	UniProt	Localization	Motif
Mitotic checkpoint serine/threonine-protein kinase BUBR1	*BUB1B*	*O60566*	Cyto/Nucleus	*LSPIiE*
RepoMan	*CDCA2*	*Q69YH5*	Nucleus	*LSPIpE*
Very large A-kinase anchor protein (vIAKAP)	CRBG3	Q69YH5	n/a	LSPIyE
Synaptopodin	SYNPO	Q8N3V7	Cell Junction	LSPIkE
Oxidation Resistance Protein 1	OXR1	Q8N573	Mitochondria	LSPIrE
Inhibitor of ASPP protein	iASPP	Q8WUf5	Cyto/Nucleus	LSPItE
Remodeling and spacing factor	RSF1	Q96T23	Nucleus	LSPIpE
Zinc finger protein 541	ZN541	Q9H0D2	Nucleus	LSPIrE
Homeobox protein nkx-2.4 (NK-2 homolog D)	NKX24	Q9H2Z4	Nucleus	LSPIeE
Uncharacterized protein KIAA1107	K1107	Q9UPP5	n/a	LSPIyE

*proteins in *italics* contain confirmed LSPIxE SLiMs that bind directly to B56

Table S4: **Number of human sequences identified in the UniProt database using increasingly less restrictive LSPIxE motifs. Related to Figure 3.**

Search Motif	Hits	Filter*	Search Motif	Hits	Filter*
[L]SP[I]	161				
[L]SP[I]xE	13	10	[L][ST]P[I]xE	18	11
[LCVM]SP[I]xE	26	15	[LCVM][ST]P[I]xE	33	17
[LCVMIF]SP[I]xE	38	20	[LCVMIF][ST]P[I]xE	57	22
[LCVM]SP[ILV]xE	117	49	[LCVM][ST]P[ILV]xE	206	72
[LCVMIF]SP[ILV]xE	173	67	[LCVMIF][ST]P[ILV]xE	301	92
[LCVMIF]SP[ILVM]xE	186	75	[LCVMIF][ST]P[ILVM]xE	327	104

*filter indicates those motifs in which the ser/thr residue satisfies the following two criteria (a) it is likely to be phosphorylated and (b) it is predicted to be in a IDR

Table S5: Excel Table of all 104 proteins identified using the following search motif: [LCVMIF][ST]P[ILVM]xE. Related to Figure 3.

Supplemental Experimental Procedures

Cloning and expression. Human B56γ1 (B56γ_{12-380} and B56γ_{31-380}) was sub-cloned into pRP1b vector (Peti and Page, 2007). B56γ_{12-380} and B56γ_{31-380} were expressed in *E. coli* BL21 (DE3) (Agilent). Cells were grown in Luria Broth in the presence of selective antibiotics at 37°C to an OD_{600} of ~0.8, and expression was induced by the addition of 0.5 mM isopropyl β-D- thiogalactoside (IPTG). Induction proceeded for ~18-20 h at 18°C prior to harvesting by centrifugation at 6,000 ×*g*. Cell pellets were stored at -80°C until purification. All peptides were synthesized, HPLC purified (>95% purity) and analyzed (MS) by Bio-Synthesis (Lewisville, TX).

Protein Purification. B56γ cell pellets were resuspended in ice-cold lysis buffer (50 mM Tris pH 8.0, 0.5 M NaCl, 5 mM imidazole, 0.1% Triton X-100 containing EDTA-free protease inhibitor tablet [Roche]), lysed by high-pressure cell homogenization (Avestin C3 Emulsiflex) and centrifuged (35,000 ×*g*, 40 min, 4°C). The supernatant was loaded onto a HisTrap HP column (GE Healthcare) pre-equilibrated with Buffer A (50 mM Tris pH 8.0, 500 mM NaCl and 5 mM imidazole) and was eluted using a linear gradient of Buffer B (50 mM Tris pH 8.0, 500 mM NaCl, 500 mM imidazole). Fractions containing the protein were pooled and dialyzed overnight at 4 °C (50 mM Tris pH 8.0, 500 mM NaCl) with TEV protease to cleave the His_6-tag. The cleaved protein was incubated with Ni^{2+}-NTA beads (GEHealthcare) and the flow-through collected. The protein was concentrated and purified using size exclusion chromatography (SEC; Superdex 75 26/60 [GE Healthcare]) pre-equilibrated in ITC Buffer (50 mM sodium phosphate pH 7.5, 300 mM NaCl, 0.5 mM TCEP) or Crystallization Buffer (20 mM HEPES pH 7.8, 500 mM NaCl, 0.5 mM TCEP). Fractions were pooled, concentrated to designated concentration for experiments or stored at -80˚C.

Crystallization and structure determination. Pooled B56γ_{31-380} (hereafter, B56) in 20 mM HEPES pH 7.8, 500 mM NaCl, 0.5 mM TCEP was concentrated and combined with *pS*-BubR1, *pSpS*-BubR1 and *pS*-RepoMan dissolved in the same buffer at a 1:5 molar ratio to a final concentration of 10 mg/ml. Initial crystals of the complexes were identified in 0.1 M HEPES pH 7.75, 0.8 M LiCl and 8% PEG6K (B56:*pS*-BubR1) or 8% PEG8K (B56:*pSpS*-BubR1, B56:*pS*-RepoMan) using hanging drop vapor diffusion at RT. Layered crystals grew overnight. Microseeding was necessary to generate single crystals. Crystals were cryo-protected by a 30 sec soak in mother liquor with 30% glycerol and immediately flash frozen. Data for the three complexes were collected at SSRL beamline 12.2 at 100 K and a wavelength of 0.98 Å using a Pilatus 6M PAD detector. The data were processed using Xds (Kabsch, 2010), Aimless (Evans and Murshudov, 2013) and Truncate (French and Wilson, 1978). The structure of B56:*pS*BubR1 was solved by molecular replacement using Phaser (Zwart et al., 2008), using B56 (PDBID 2JAK) as the search model (Magnusdottir et al., 2009). A solution was obtained in space group $P2_12_12_1$; clear electron density for the BubR1 peptide was visible in the initial maps. The initial models of the complex were built without the peptide using AutoBuild, followed by iterative rounds of refinement in PHENIX and manual building using Coot (Emsley et al., 2010). The peptide coordinates were then added followed by iterative rounds of refinement in PHENIX and manual building using Coot. The remaining complexes were phased using Fourier synthesis and refined in similar fashion. Data collection and refinement details are provided in **Table 1**.

Isothermal titration calorimetry. SEC was performed to polish B56 and exchange into ITC Buffer (50 mM sodium phosphate pH 7.5, 300 mM NaCl, 0.5 mM TCEP). BubR1 (70-100 μM) or RepoMan (70-100 μM) peptides were titrated into B56γ_{12-380} (7-10 μM) using a VP-ITC micro-calorimeter at 25°C (Malvern). Data were analyzed using NITPIC, SEDPHAT and GUSSI (Scheuermann and Brautigam, 2015; Zhao et al., 2015).

Bioinformatics. Multiple methods were used to confirm that the identified motifs are present in IDPs. First, IUPRED was used to distinguish sequences likely folded (IUPRED scores ≤0.4) from those likely disordered (IUPRED score> 0.4) (Dosztanyi et al., 2005). The 126 sites identified to be present in IDPs using IUPRED were then subsequently examined using both DisEMBL (loops/coils definition) (Linding et al., 2003) and PONDR (using both the VL3-BA and the VLXT predictors) (Romero et al., 2001). This resulted in a total of 102 sites classified as disordered by all three prediction algorithms with 24 sites predicted to be disordered by only 1 or 2 algorithms. The latter sites were investigated for (a) their presence in the PDB, (b) the presence of distal homologs whose structures are known (FFAS) (Xu et al., 2014) and (c) the likelihood that they are present in transmembrane domains or in coiled-coils. This additional analysis resulted in 2 of the 24 sites classified as disordered. The remaining 22 sites were eliminated as their sequences were present in protein domains that are structured, structures had been determined or proteins classified as secreted.

The ConSurf server (using 150 unique B56 sequences with the lowest E values (Ashkenazy et al., 2010)) were used to calculate the conservation scores. Figures generated using PYMOL. The T-Coffee Multiple Sequence Alignment Server (Notredame et al., 2000) was used to generate the sequence alignment for B56 isoforms and splice variants. Multiple Align Show (www.bioinformatics.org/sms/multi_align.html) was used to enhance the output from T-Coffee.

Supplemental References

Ashkenazy, H., Erez, E., Martz, E., Pupko, T., and Ben-Tal, N. (2010). ConSurf 2010: calculating evolutionary conservation in sequence and structure of proteins and nucleic acids. Nucleic Acids Res *38*, W529-533.

Dosztanyi, Z., Csizmok, V., Tompa, P., and Simon, I. (2005). The pairwise energy content estimated from amino acid composition discriminates between folded and intrinsically unstructured proteins. J Mol Biol *347*, 827-839.

Emsley, P., Lohkamp, B., Scott, W.G., and Cowtan, K. (2010). Features and development of Coot. Acta Crystallogr D Biol Crystallogr *66*, 486-501.

Evans, P.R., and Murshudov, G.N. (2013). How good are my data and what is the resolution? Acta Crystallogr D Biol Crystallogr *69*, 1204-1214.

French, G.S., and Wilson, K.S. (1978). On the treatment of negative intensity observations. Acta Crystallogr A *34*, 517-525.

Kabsch, W. (2010). Xds. Acta Crystallogr D Biol Crystallogr *66*, 125-132.

Linding, R., Jensen, L.J., Diella, F., Bork, P., Gibson, T.J., and Russell, R.B. (2003). Protein disorder prediction: implications for structural proteomics. Structure *11*, 1453-1459.

Magnusdottir, A., Stenmark, P., Flodin, S., Nyman, T., Kotenyova, T., Graslund, S., Ogg, D., and Nordlund, P. (2009). The structure of the PP2A regulatory subunit B56 gamma: the remaining piece of the PP2A jigsaw puzzle. Proteins *74*, 212-221.

Notredame, C., Higgins, D.G., and Heringa, J. (2000). T-Coffee: A novel method for fast and accurate multiple sequence alignment. J Mol Biol *302*, 205-217.

Peti, W., and Page, R. (2007). Strategies to maximize heterologous protein expression in Escherichia coli with minimal cost. Protein Expr Purif *51*, 1-10.

Romero, P., Obradovic, Z., Li, X., Garner, E.C., Brown, C.J., and Dunker, A.K. (2001). Sequence complexity of disordered protein. Proteins *42*, 38-48.

Scheuermann, T.H., and Brautigam, C.A. (2015). High-precision, automated integration of multiple isothermal titration calorimetric thermograms: new features of NITPIC. Methods *76*, 87-98.

Xu, D., Jaroszewski, L., Li, Z., and Godzik, A. (2014). FFAS-3D: improving fold recognition by including optimized structural features and template re-ranking. Bioinformatics *30*, 660-667.

Zhao, H., Piszczek, G., and Schuck, P. (2015). SEDPHAT--a platform for global ITC analysis and global multi-method analysis of molecular interactions. Methods *76*, 137-148.

Zwart, P.H., Afonine, P.V., Grosse-Kunstleve, R.W., Hung, L.W., Ioerger, T.R., McCoy, A.J., McKee, E., Moriarty, N.W., Read, R.J., Sacchettini, J.C.*, et al.* (2008). Automated structure solution with the PHENIX suite. Methods Mol Biol *426*, 419-435.